processes

MDPI

Article

Study on Structure Dynamic Characteristics for Internal Components of Kaplan Turbine Runner under Different Contact Modes

Chengming Liu [1], Haiqiang Luo [2], Guiyu Wang [2], Xiaobin Chen [2], Lingjiu Zhou [1] and Zhengwei Wang [3,*]

[1] College of Water Resources and Civil Engineering, China Agricultural University, Beijing 100083, China; lamous3006@163.com (C.L.)
[2] Guangxi Datengxia Gorge Water Conservancy Development Co., Ltd., Guiping 537226, China; sdgc11@163.com (G.W.); leihuai2006@163.com (X.C.)
[3] State Key Laboratory of Hydroscience and Engineering, Department of Energy and Power Engineering, Tsinghua University, Beijing 100084, China
* Correspondence: wzw@mail.tsinghua.edu.cn

Abstract: The stress and fatigue of the runner during the operation of the large Kaplan turbine are one of the key issues in the operation of turbines. Due to the complexity of the working load and the geometric configuration of the Kaplan turbine runner, the different contact modes between the internal components of the runner will have an impact on the stress and fatigue results. Therefore, the unsteady CFD calculation of the full channel is conducted in this article to analyze the hydraulic characteristics of the turbine blades in the unsteady flow field, such as pressure and torque. The pressure load is loaded onto the runner using a fluid–structure interaction (FSI) theory, and the stress characteristics of the blade, blade lever, and runner body are compared under three contact modes. Based on the dynamic stress spectrum of the blade lever calculated under three contact conditions, the life of the blade lever is predicted using the rain flow counting method and the Palmgren–Miner theory. The results indicate that the rotation of the runner has a significant impact on the hydraulic and structural characteristics of the Kaplan turbine. The non-uniform and asymmetric stress and torque conditions gradually cause fatigue in the components of the runner. The average and amplitude of dynamic stress on the blade, blade lever, and runner body under frictional and frictionless contact are greater than those of fixed contact. The life of the blade lever calculated under fixed contact is much greater than that under frictional and frictionless contact; therefore, the contact conditions have a significant impact on the structural characteristics of the runner.

Keywords: torque; rain flow counting method; blade lever; Kaplan turbine; fluid–structure interaction

Citation: Liu, C.; Luo, H.; Wang, G.; Chen, X.; Zhou, L.; Wang, Z. Study on Structure Dynamic Characteristics for Internal Components of Kaplan Turbine Runner under Different Contact Modes. *Processes* **2024**, *12*, 1061. https://doi.org/10.3390/pr12061061

Academic Editor: Krzysztof Rogowski

Received: 22 March 2024
Revised: 13 May 2024
Accepted: 19 May 2024
Published: 22 May 2024

1. Introduction

In recent years, the trend toward reducing carbon emissions has become increasingly strong. As a renewable energy industry, hydropower has developed rapidly in order to meet this demand. Among them, the Kaplan turbine is widely used in various low-head rivers due to its characteristics of a large flow rate and low head [1]. The runner of Kaplan turbines contains many components. When the operating conditions change, the flow rate can be adjusted by changing the blade angle [2]. Therefore, the internal components of the impeller are often subjected to more stress and vibration. During the continuous rotation of the runner, the structure is subjected to periodic loads, resulting in fatigue losses. Due to changes in climate conditions and electricity consumption, the Kaplan turbine often operates under non-design conditions such as high flow conditions, causing unit vibration and significant pressure pulsation [3–5]. At the same time, it causes significant changes in the stress of the internal components of the impeller and increases the fatigue loss of the turbine [6–8]. It is inevitable that losses and gaps will occur and even lead to the fracture of key parts such as blades, blade levers, and piston rods [9].

Under high flow conditions, the output of the turbine is greater, and the torque received by the blades is greater [10–12]. The stress and loss transmitted to the internal components of the runner through the blades will also increase. The axial flow fixed blade turbines of China's Hongshi Power Station [13] and the first turbine of the Sulya Dishlin Hydropower Station [14] have both experienced varying degrees of cracks in their runner blades since their grid connection. After prolonged operation, the internal components of the runner may even be damaged or broken. In order to repair this equipment, the crew had to shut down the equipment and spend a lot of time repairing it, resulting in a significant loss of manpower and financial resources. Therefore, it is necessary to conduct dynamic stress, fatigue analysis, and structural life calculations in advance and predict and prevent potential hazards.

In order to address the fatigue problem of water turbine blades, extensive research has been conducted, and certain research results have been achieved [15,16]. The most common approach is to equate the stress and strain of the structure, assuming that the equivalent uniaxial stress amplitude is the same as the fatigue damage caused by multiaxial stress [17–19]. Equivalent stress is considered a control parameter for the material damage process. Then, the random fatigue stress loads borne by the turbine structure are compiled into a load spectrum that can simulate the real stress situation [20]. This serves as the load basis for theoretical analysis and fatigue testing. At present, the rain flow counting method is mainly used to process the stress time history and obtain an array of stress means and amplitudes.

The fatigue of Kaplan runners is influenced by various factors, such as connection methods and load characteristics [21], and the relationship between different factors is very complex. Therefore, there is still a lack of research on the mechanism and specific hazards of fatigue generation in this multi-body structure [22]. At present, there are two main forms of research on the dynamic stress of Kaplan turbines: experimental and numerical simulation. Numerical simulation mainly uses the method of FSI to connect different components inside the runner in the form of contact elements for calculation. Due to the important role of the interaction between contact components in the efficient and stable operation of the runner, different contact relationships will have an impact on the dynamic stress results and service life of the Kaplan turbine.

In this article, the hydraulic characteristics of the Kaplan turbine in a certain hydropower station under high flow conditions, such as pressure and torque, are studied and calculated. Then, the dynamic stress characteristics and fatigue life analysis of fixed contact, frictional contact, and frictionless contact between the components of the runner are studied. The life of the blade lever under different contact relationships is calculated.

2. Numerical Calculation Methods

2.1. Model

In this article, a computational fluid dynamics (CFD) model is used to calculate the full flow of a Kaplan turbine, and then a finite element model (FEM) is used to calculate the structural field of the Kaplan turbine. The entire computational flow field of a Kaplan turbine includes the spiral case, guide vanes, stay vanes, runner, and draft tube, as shown in Figure 1. The solid part of the Kaplan turbine consists of blades, a runner body, blade levers, blade links, bolts, a piston rod, and others, as shown in Figure 2.

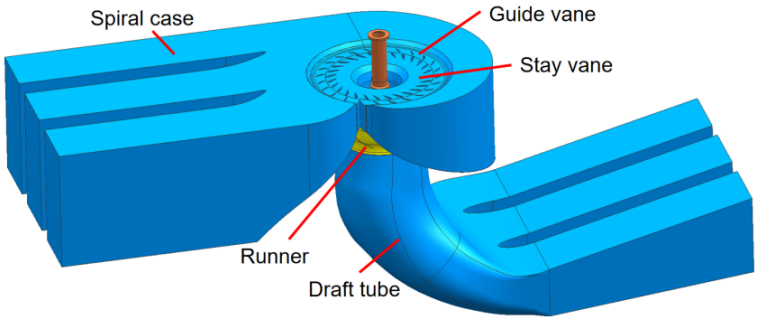

Figure 1. Fluid domain model.

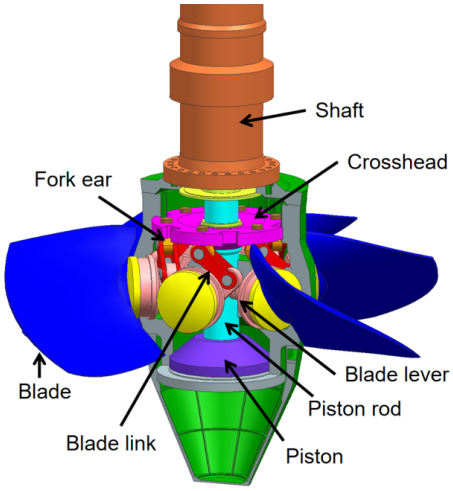

Figure 2. Internal structure of the runner.

2.2. Calculation of Flow Field

In this article, the transient flow characteristics of the flow field were obtained through commercial ANSYS 19.1 CFX and then imported into ANSYS APDL 19.1 to obtain the dynamic response characteristics of the runner structure. In the calculation of flow fields, the Reynolds-averaged Navier–Stokes (RANS) equation is mainly used [23]. The turbulence model is the SST $k-\omega$ model, which has high accuracy in calculating turbulent shear stress and can effectively predict the size of the separation zone at the separation point under a reverse pressure gradient [24]. In this fluid calculation, the rated head of the Kaplan turbine is 25 m, the inlet of the spiral case is set as a full-pressure inlet, and the outlet of the draft tube is set as a static pressure outlet. The rotational speed of the runner domain is set to 68.2 r/min, while the other fluid domains are set to static. All walls are set to no-slip. The time step is set to 1/126 of the rotation period. The parameters are shown in the Table 1 below.

Table 1. Parameters of Kaplan turbine.

Parameter	Value
Rotating speed of the rotor n	68.2 r/min
Number of stay vanes Zs	25
Number of guide vanes Zg	28
Number of blades Zr	6
Diameter of the rotor D	10.4 m
Head H	25 m
Paddle angle (°)	6.078
Angle of guide vane (°)	48.1

2.3. Finite Element Model

In the FEM simulation, FSI is used to study the blade stress and strength of the Kaplan turbine. The force results of the three-dimensional CFX fluid calculation are calculated, and these acceptance results are used as external loads applied to the runner. The time step in FSI calculation is the same as that in flow field calculation, with a rotation period of 1/126, and a total of 3 rotation periods are calculated. The solution of the solid domain is based on linear dynamic equilibrium equations, which can be expressed in discrete form as [25]:

$$[M]\{\ddot{u}\} + [C]\{\dot{u}\} + K\{u\} = \{F\} \quad (1)$$

Among them, $[M]$, $[C]$, and $[F]$ are the mass matrix, damping matrix, and stiffness matrix. $\{\ddot{u}\}$,$\{\dot{u}\}$,$\{u\}$ represents acceleration, velocity, and displacement. $[F]$ is a node load vector determined by the gravity, centrifugal force, and hydraulic pressure on the FSI boundary.

2.4. Mesh of Flow Field

The fluid domain in this article is mainly divided into tetrahedral elements with good adaptability. Due to the significant impact of the number of meshes on the accuracy of calculation results, the efficiency of Kaplan turbines under rated operating conditions is used to verify the independence of flow field meshes. Comparing the calculation results of different sets of meshes with experimental values, the verification results of grid independence are shown in Figure 3. When the number of mesh nodes is less than 5.54 million, the efficiency shows a clear upward trend. When the total number of mesh nodes exceeds 5.54 million, the calculated efficiency remains basically unchanged, and the difference between the calculated efficiency of 92.9% and the experimental efficiency of 93.1% is small. On the premise of ensuring the cost and accuracy of the calculation, the set of 5.54 million meshes is selected for this calculation, as shown in Figure 4. The number of meshes for different fluid domains is shown in Table 2.

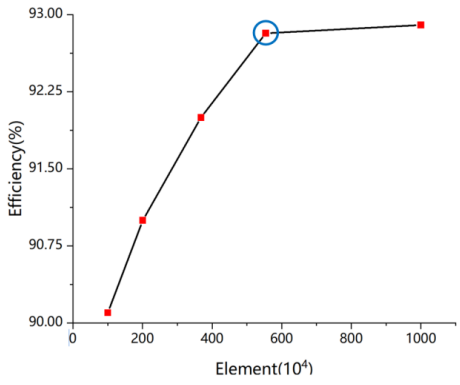

Figure 3. Mesh independence test.

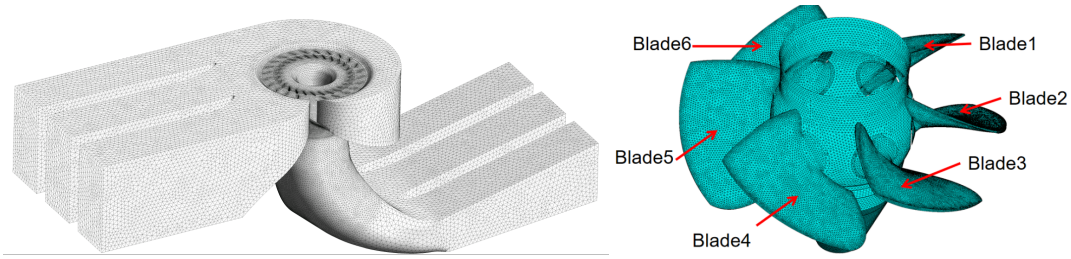

(**a**) Mesh of flow field (**b**) Mesh on the surface of the runner

Figure 4. Mesh.

Table 2. Number of mesh elements for each flow channel (10^4).

Flow Channel	Set 1	Set 2	Set 3	Set 4	Set 5
Spiral case	12	23	45	65	131
Stay vane	14	28	52	73	147
Guide vane	23	46	78	83	150
Runner	30	61	140	253	490
Draft tube	21	45	71	80	114
Total	101	203	386	554	1032

2.5. Structural Field Mesh

The solid domain model of the runner is divided into ANSYS Mesh. Hexahedral mesh is used on the shaft, while tetrahedral mesh is used on structures such as blades, a piston, and a crosshead. For the verification of mesh independence in the solid domain, the maximum stress of blades with different mesh numbers is calculated in this paper. When the number of runner elements is 1.55 million, the maximum stress on the blade is 149 MPa, which is only 0.5% different from that of the 2.34 million mesh elements. Therefore, the solid domain is divided into 1.55 million elements. The boundary conditions for the runner are set according to the actual situation. As is shown in Figure 5. Fixed support is applied to the upper surface of the shaft and the lower surface of the piston rod, and the interface between the shaft and the thrust bearing is set as a frictionless interface. The interaction surface between the blades and the flow is set as the fluid–structure coupling surface. In this study, the main focus is on analyzing the impact of the unsteady characteristics of the flow field inside the Kaplan turbine on the key components of the turbine. The influence of blade deformation on the characteristic parameters and pressure pulsation characteristics of the internal flow field is limited, so the influence of blade deformation on the internal flow field is not considered. The unidirectional coupling method is adopted to calculate the dynamic stress characteristics of key components.

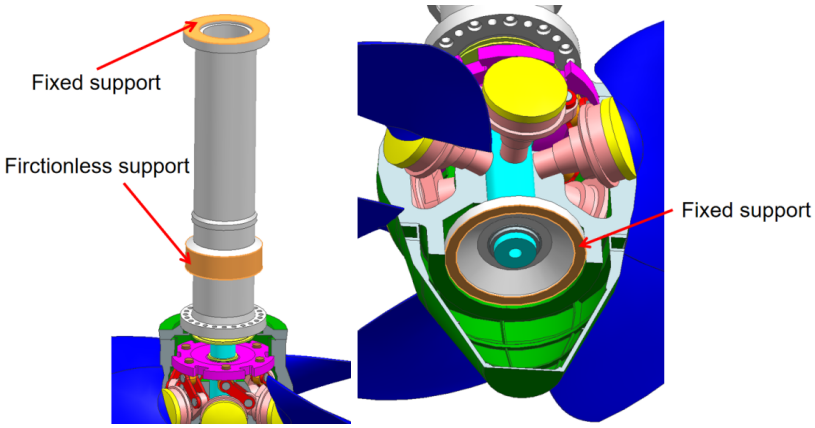

(**a**) Support on the shaft (**b**) Support on the piston rod

Figure 5. Boundary setting of the runner.

When two separated surfaces come into contact and shear each other, it is called contact. The surfaces in contact cannot penetrate each other but can transmit normal pressure and tangential friction and usually do not transmit normal tension. The contact between two faces involves multiple ways of resolving relationships. When the contact area is set to be bonded, relative sliding or separation between faces or lines is not allowed. When the contact area is set to frictionless, it represents unilateral contact. If separation occurs, the normal pressure is zero. When the contact area is set to frictional, the two contact surfaces can transmit a certain amount of shear stress through the contact area before relative sliding occurs. The model defines an equivalent shear stress as part of the contact pressure before sliding occurs. Once the shear stress exceeds this value, relative sliding will occur on both

sides. Frictionless and frictional contact are nonlinear contacts, while bonded contact is linear contact. The Kaplan turbine runner is a multi-body structure consisting of multiple components such as blades, pistons, and operating rods. The complex contact relationships between each component have a significant impact on the dynamic stress characteristics of FSI. Therefore, in this article, the dynamic stress response characteristics and fatigue life analysis of the runner are studied by setting the contact relationship of all components of the runner as bonded, frictional, and frictionless. The main contact surfaces are shown in Figure 6. The blue face is the target face, and the red face is the contact face.

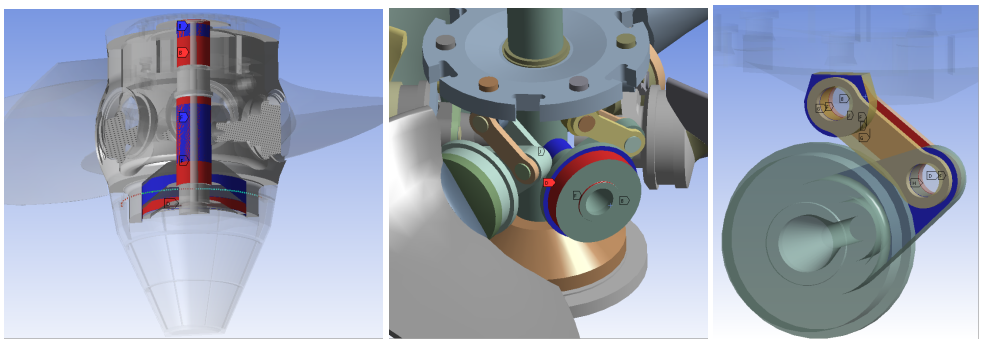

(**a**) Piston rod (**b**) Blade lever (**c**) Blade link

Figure 6. Contact relationship of runner components.

3. Flow Field Analysis

3.1. Pressure Characteristics

Pressure monitoring points are arranged on the wall surface of the vaneless area of the turbine, the pressure surface of the runner blades, and the wall surface of the draft tube. The positions of GV and DT are fixed, while RU rotates with the rotation of the blades. The monitoring point positions are shown in Figure 7. Figure 8 shows the the spectrum of RU and time-history results of pressure pulsation at GV1, RP1, and DT1. It can be seen that the pressure gradually decreases along the channel, and the pressure fluctuation value of RU is significantly greater than that of the other two points. Due to the rotation of the RU point with the runner, the main frequency of RU is 1fn, and its amplitude is 1.27 kPa. Figure 9 shows the pressure distribution on the surface of the runner blades. The leading edge of the blade pressure surface has a small range of low-pressure areas, while the leading edge of the blade suction surface has a small range of high-pressure areas.

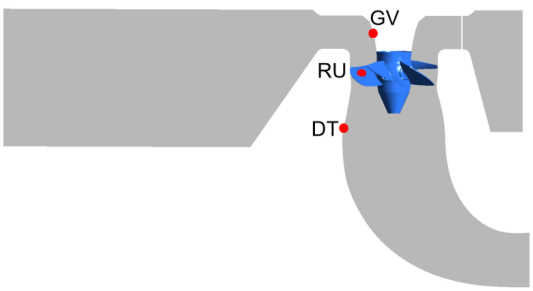

Figure 7. Pressure monitoring points.

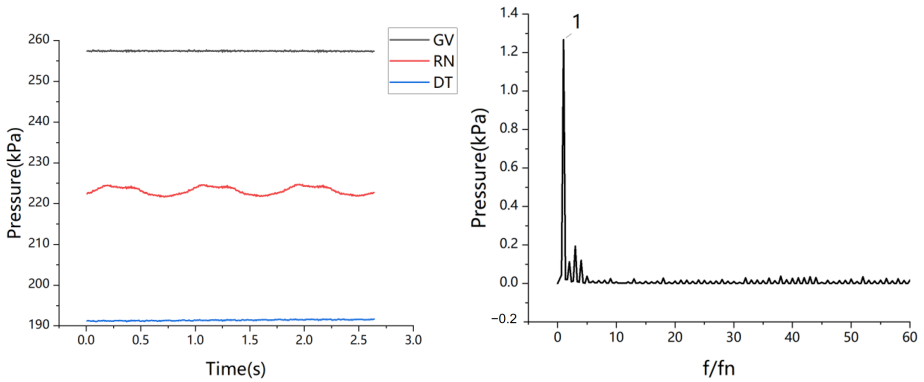

(**a**) Time domain of pressure monitoring points (**b**) The pressure frequency domain of RU

Figure 8. Pressure monitoring point results.

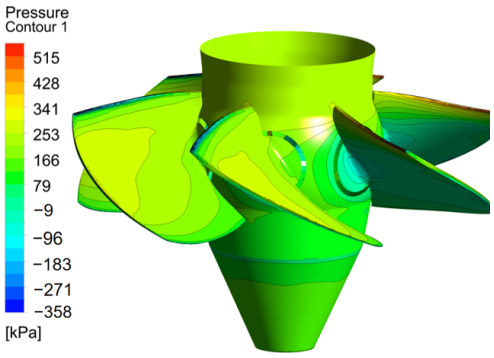

Figure 9. Pressure on the surface of the runner.

3.2. Torque

Figure 10a shows the time-domain of torque for six blades. It can be seen that the torque fluctuates periodically, and the maximum and minimum torque values of different blades are different. The torque difference between different blades at the same time is significant. Figure 10b shows the frequency domain of torque for six blades, with almost identical pulsation amplitudes for torque across different blades. The main frequency of torque for all blades is 1 fn, which is the same as the main frequency of pressure pulsation, with an amplitude of 0.94 × 10^4 N·m. The torque of the runner blades around their own blade lever is ultimately transmitted to other components inside the runner through the blades. The unevenly distributed and constantly changing torque will ultimately have a significant impact on the fatigue of the runner components.

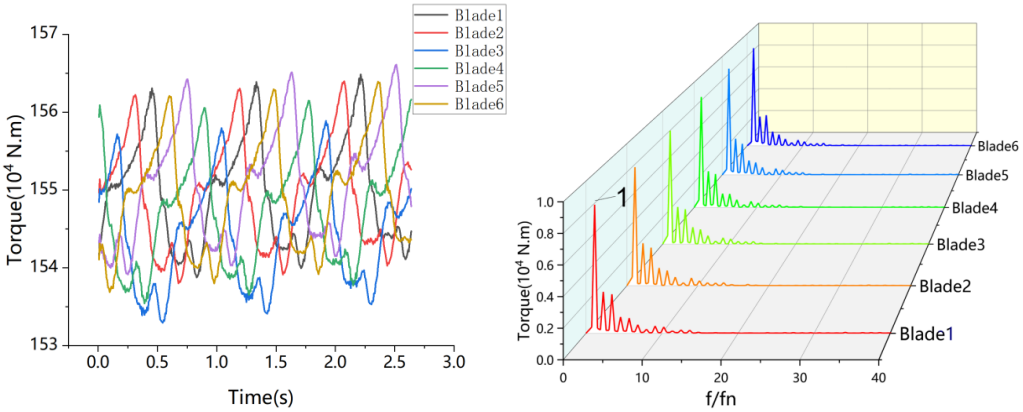

(**a**) Time domain of torques (**b**) Frequency domain of torques

Figure 10. Time and frequency domain of torques.

4. Displacement

Displacement Distribution

Figure 11 shows the displacement distribution under three contact modes. The maximum displacement of the three contact modes occurs at the outer edge of the blade, near the runner outlet. The displacement results of fixed contact are smaller than those of the other two contact conditions. Under fixed contact conditions, there is almost no displacement on the hub of the runner body, while the hub surface in frictional and frictionless contact will experience displacement. The maximum displacement of fixed contact is 0.142 m, the maximum displacement of frictional contact is 0.238 m, and the maximum displacement of frictionless contact is 0.231 m. It can be seen that the displacement of the runner body calculated by the three types of contact differs greatly. The time history curve and frequency domain curve of the maximum displacement point on the blade are shown in Figure 12. It can be seen that the main frequency amplitude of displacement pulsation of the blade is similar under the three contact conditions, all of which are around 0.4 mm. The main vibration frequency of the three types of contact is 1 times the rotational frequency (1.136 Hz), which is related to the rotation of the runner, indicating that the rotation of the runner has a significant impact on the displacement of the blades.

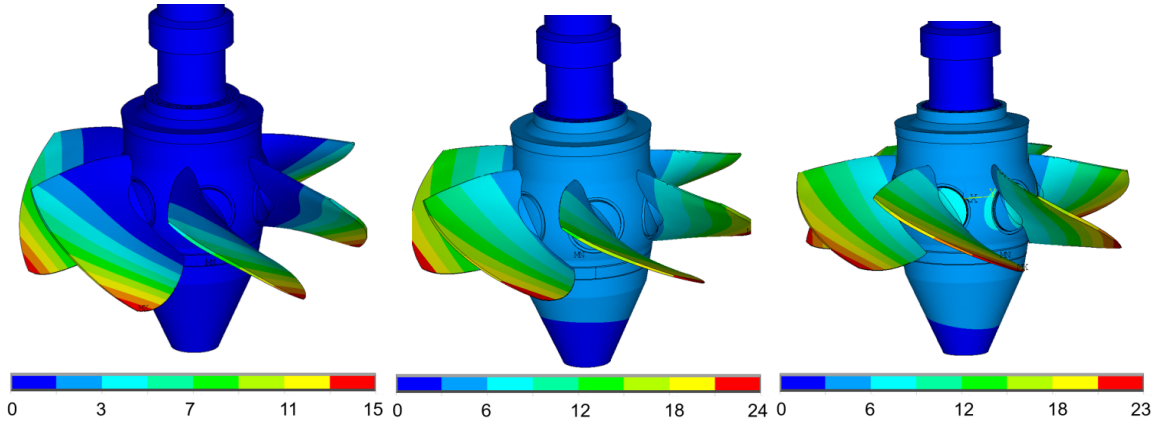

(**a**) Bonded contact (**b**) Frictional contact (**c**) Frictionless contact

Figure 11. Displacement distribution of the runner under three contact modes.

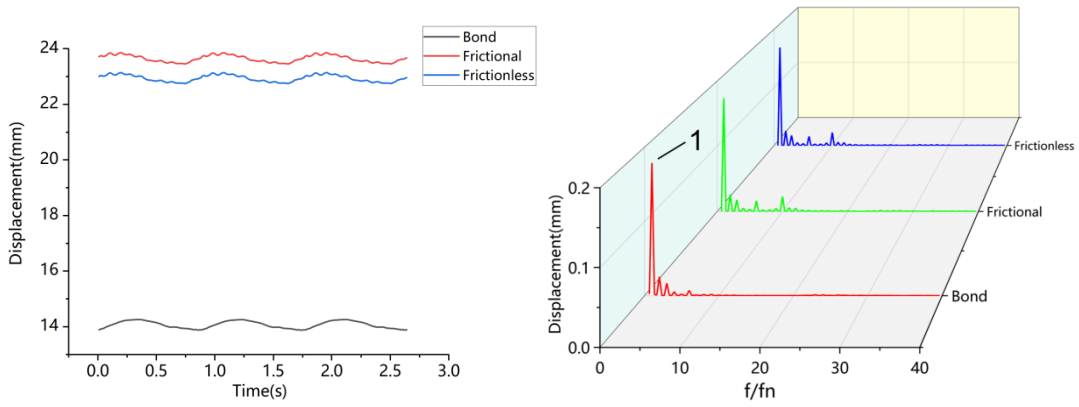

(**a**) Time domain (**b**) Frequency domain

Figure 12. Time and frequency domain analysis of the maximum displacement point of the runner under three contact modes.

5. Stress

5.1. Stress Analysis of Runner Blades

Figure 13 shows the stress distribution of the blade under three contact conditions. It can be seen that the maximum stress on the blade under the three contact conditions is

located at the root of the blade near the runner outlet side. The stress in frictional contact and frictionless contact is similar and greater than that in fixed contact. Figure 14 shows the dynamic stress time-domain and frequency-domain diagrams of the maximum stress node on the blade under three different conditions. The average stress at the maximum stress node on the fixed contact blade is 193 MPa, with a main frequency of 1 fn and an amplitude of 2.55 MPa. The average stress at the maximum stress node on the blade in frictional contact is 233 MPa, with a main frequency of 1 fn and an amplitude of 1.77 MPa. The average stress at the maximum stress node on the blade without frictional contact is 230 MPa, with a main frequency of 1 fn and an amplitude of 1.75 MPa. It can be seen that under different contact conditions, the mean and amplitude of dynamic stress at the nodes on the blade do not change much, and the main frequency of dynamic stress pulsation is the same as that of pressure pulsation.

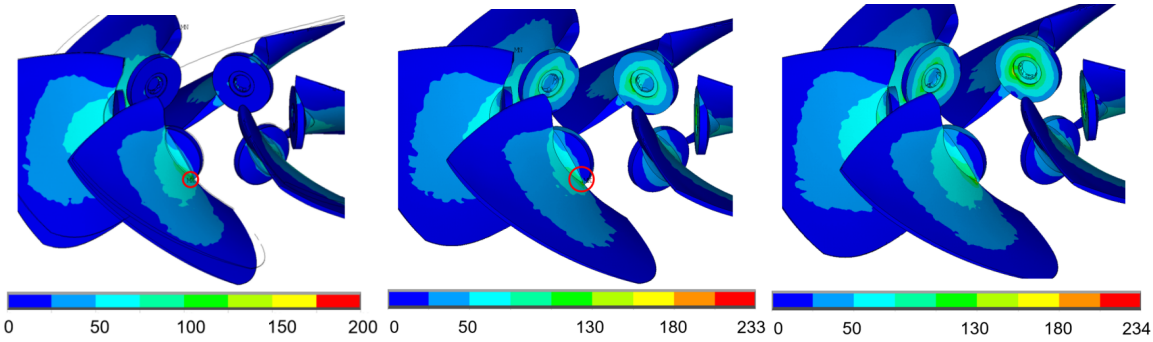

(**a**) Bonded contact (**b**) Frictional contact (**c**) Frictionless contact

Figure 13. Stress of blade under three contact modes.

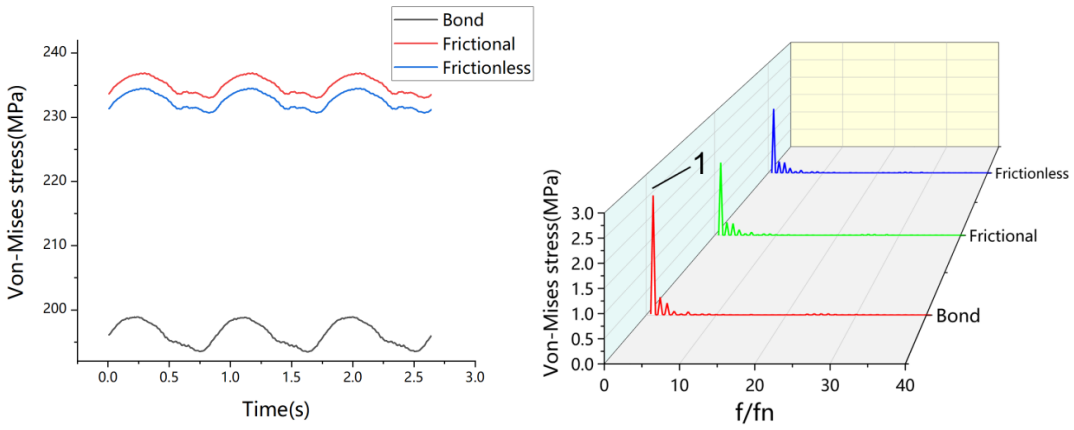

(**a**) Time domain (**b**) Frequency domain

Figure 14. Time and frequency domain of the maximum stress point of the blade under bonded contact.

5.2. Stress Analysis of Blade Levers

Figure 15 shows the distribution of blade lever stress under three contact conditions. It can be seen that the stress distribution of the blade lever in frictional contact and frictionless contact is similar, but there is a significant difference compared to that of fixed contact. The maximum stress on the blade lever under fixed contact is located at the connection between the blade lever and the inner surface of the runner body. The maximum stress on frictional and frictionless contact is located at the junction of the blade lever and the inner surface of the hub. The stress at the connection between the blade lever and the blade link is significantly higher under friction and frictionless contact. Figure 16 shows the dynamic stress time and frequency domains of the maximum stress node on the blade lever in three different modes. The average stress at the maximum stress node under the

fixed contact mode is 19.6 MPa, with a pulsating frequency of 1 fn and an amplitude of 0.178 MPa. The average stress at the maximum stress node under the friction contact mode is 305 MPa, with a pulsation frequency of 1 fn and an amplitude of 4.14 MPa. The average stress at the maximum stress node under the frictionless contact mode is 299 MPa, with a pulsating frequency of 1 fn and an amplitude of 4.09 MPa. Therefore, there is a significant difference in the mean and amplitude of dynamic stress at the nodes on the blade lever under different contact conditions. The dynamic stress and pulsation values on the blade lever of frictional contact and frictionless contact are significantly greater than those of the fixed contact.

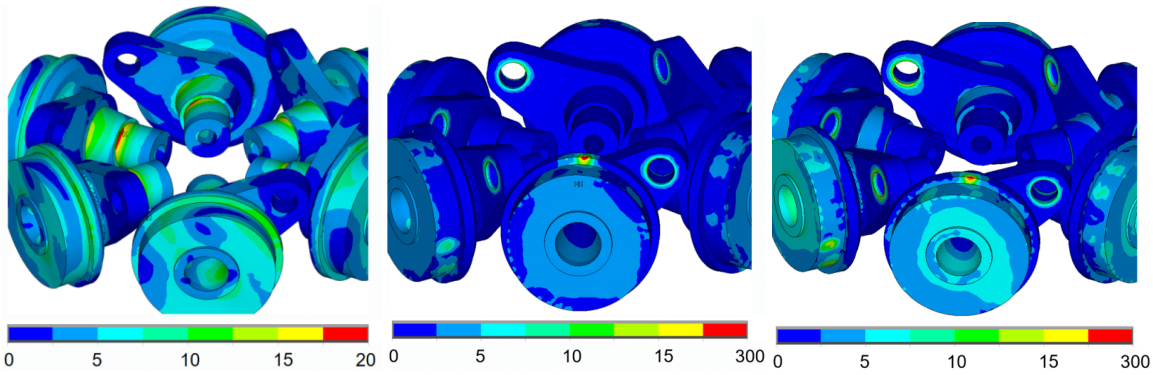

(**a**) Bonded contact (**b**) Frictional contact (**c**) Frictionless contact

Figure 15. Stress of blade lever under three contact modes.

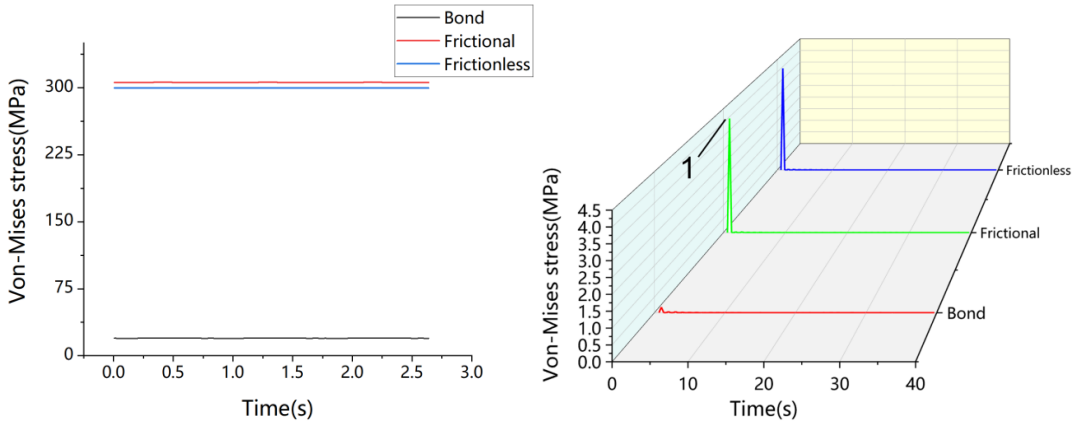

(**a**) Time domain (**b**) Frequency domain

Figure 16. Time and frequency domain of the maximum stress point of the blade lever under frictional contact.

5.3. Stress Analysis of Runner Body

Figure 17 shows the stress distribution of the runner body under three contact conditions. Under all three types of contact, the stress is relatively high at the junction of the blade and the hub, but the stress distribution on the hub surface of the fixed contact is significantly different from that of the other two modes. The stress on the outer surface of the hub increases significantly under friction and frictionless contact modes, and the stress reaches its maximum value at the junction of the blade lever circumference surface and the hub of the runner body. The dynamic stress time-domain and frequency-domain diagrams of the maximum stress node on the runner body under three contacts are shown in Figure 18. The average stress at the maximum stress node on the runner body under fixed contact is 42 MPa, with a main frequency of 1 fn and an amplitude of 0.456 MPa. The average stress at the maximum stress node on the runner body under frictional contact is 248 MPa, with a main frequency of 1 fn and an amplitude of 3.83 MPa. The average stress

of the maximum stress node under frictionless contact is 244 MPa, with a main frequency of 1 fn and an amplitude of 3.8 MPa. The stress and pulsation of the runner body under frictional contact and frictionless contact are much greater than those under fixed contact.

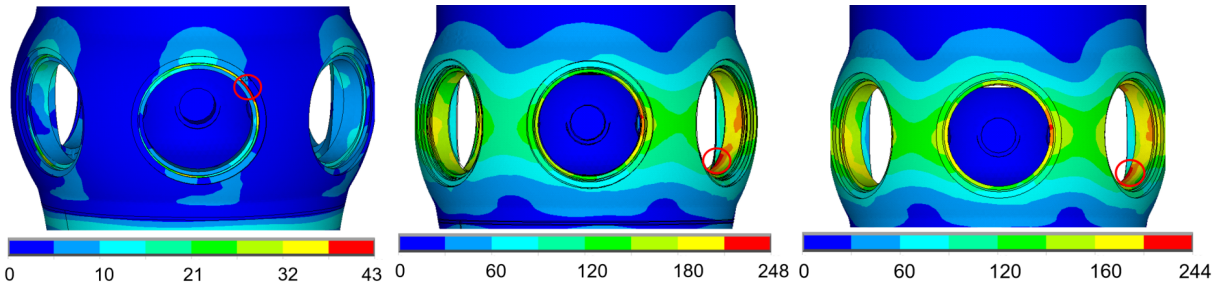

(**a**) Bonded contact (**b**) Frictional contact (**c**) Frictionless contact

Figure 17. Stress of runner body under three contact modes.

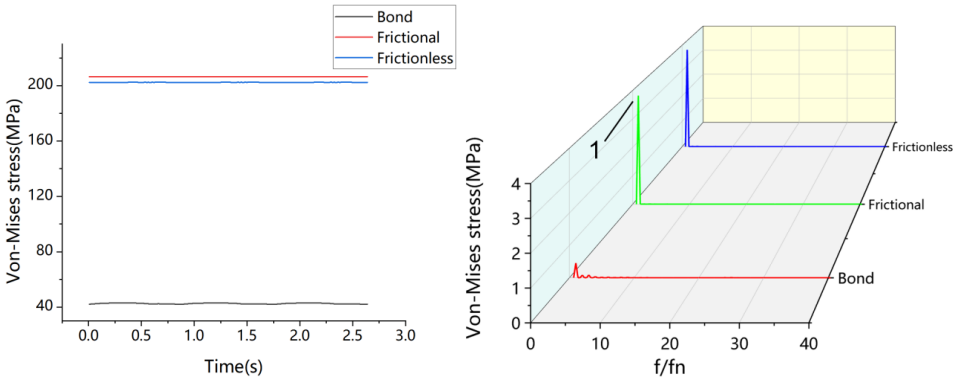

(**a**) Time domain (**b**) Frequency domain

Figure 18. Time and frequency domain of the maximum stress point of the runner body under frictional contact.

6. Calculation of the Fatigue Life

6.1. Rainflow Counting Method

The stress of the blade lever varies significantly under different contact conditions, which definitely has a significant impact on the lifespan of the blade lever. Therefore, in this article, the lifespan of the blade lever under different contact conditions is calculated and compared. The average variation range of stress load on the blade lever in water is large, so the influence of average stress variation should not be ignored in fatigue reliability design. The rain flow method belongs to the dual-parameter counting method and is currently the most widely used counting method. By controlling the binary random variables of stress mean and stress amplitude, the real stress time history is simplified into a typical load spectrum. This method establishes a certain connection between the statistical characteristics of the load and the fatigue characteristics of the material. Therefore, the rain flow counting method is adopted. A computer program is developed in Matlab (R2023a; MathWorks, Natick, MA, USA) based on the dynamic stress characteristics of the blade lever and the three-point rain flow counting method. The information on the mean stress *Sm*, amplitude *Sa*, and measured frequency of the joint grouping is obtained by processing the previous stress time, as shown in Figure 19. It is generally believed that grouping the mean stress data into 10 levels of amplitude data has sufficient accuracy.

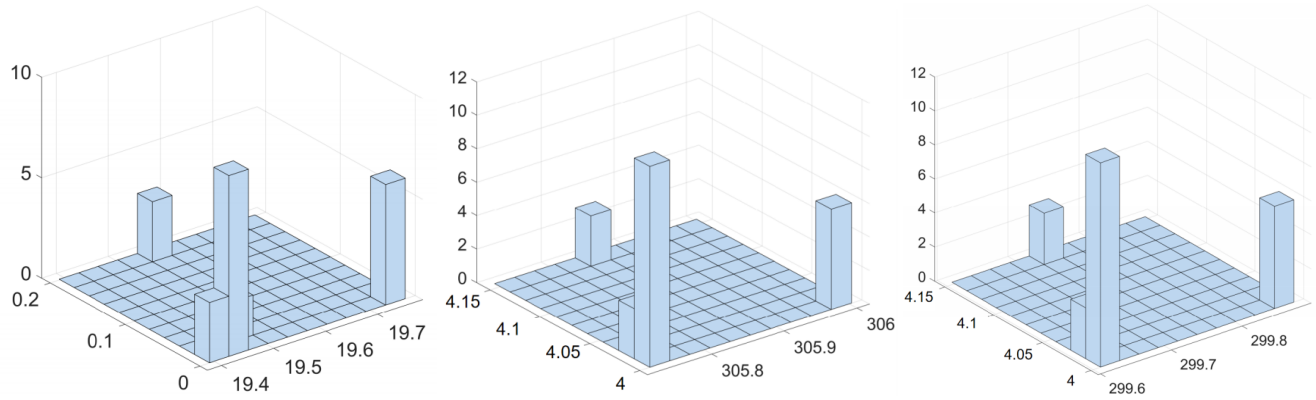

(**a**) Bonded contact (**b**) Frictional contact (**c**) Frictionless contact

Figure 19. Two dimensional fatigue stress observation frequency histogram.

6.2. Life

The fatigue characteristic curve of metal materials under alternating stress can be determined by fatigue tests. The higher the stress amplitude of the material, the lower the number of stress cycles N for fatigue failure. The material of the blade lever in this article is cast steel 35CrMo. The tensile strength σ_b of 35CrMo is 745 MPa. The yield strength σ_s is 561 MP. The fatigue strength σ_w is 388 MPa. The fatigue life prediction adopts the Basquin formula:

$$\sigma_a = 2539\left(2N_f\right)^{-0.126} \tag{2}$$

N_f is the number of cycles to failure. The different combinations between average stress and stress amplitude can result in a constant fatigue life. In this article, the Goodman equivalent life model commonly used in engineering for high cycle fatigue reliability design is used to equate various stress levels (Sa, Sm) to symmetric cycles. In this way, the stress cycle obtained by the rain flow counting method mentioned above is converted into an equivalent stress spectrum with a mean of 0. The Goodman curve formula is:

$$\frac{S_a}{\sigma_a} + \frac{S_m}{\sigma_b} = 1 \tag{3}$$

σ_a is the fatigue limit of the material under symmetric cycles. Tables 3–5 show the σ_a of the maximum stress point of the blade lever calculated under three contact conditions. In order to simplify the calculation, similar σ_a is divided together. Therefore, under the bond contact method, σ_a is divided into three parts: 0.01, 0.03, and 0.195. Under frictional contact mode, σ_a is divided into three parts: 6.81, 6.83, and 7.03. Under frictionless contact mode, σ_a is divided into three parts: 6.72, 6.74, and 6.93. Then, the lifespan and damage degree of the blade lever are calculated based on the material performance curve.

Table 3. σ_a and number of σ_a cycles of blade lever under bonded contact mode.

***Sm* (MPa)**	***Sa* (MPa)**	**σ_a (MPa)**	**Number of σ_a Cycles *n***
19.41	0.01	0.01	3
19.45	0.01	0.01	9
19.48	0.03	0.03	2
19.51	0.19	0.195	3
19.79	0.01	0.01	6

Table 4. σ_a and number of σ_a cycles of blade lever under frictional contact mode.

Sm (MPa)	*Sa* (MPa)	σ_a (MPa)	Number of σ_a Cycles *n*
305.72	4.014	6.808	12
305.72	4.028	6.831	3
305.85	4.142	7.027	3
305.99	4.014	6.812	6

Table 5. σ_a and number of σ_a cycles of blade lever under frictionless contact mode.

Sm (MPa)	*Sa* (MPa)	σ_a (MPa)	Number of σ_a Cycles *n*
299.63	4.014	6.714	12
299.63	4.028	6.738	3
299.73	4.142	6.931	3
299.87	4.014	6.718	6

The Miner criterion can effectively predict the mean life of structures under random loading. In this article, based on the Miner linear cumulative damage rule, it is believed that the fatigue damage of materials at various stress levels is independent. The total damage can be linearly superimposed, and the fatigue damage of each level of load can be represented by n_i/N_i. When the stress during the entire working period accumulates to 1, that is, when D=1, the component fails. The formula for calculating total damage is:

$$D = \sum_{i=1}^{d} D_i = \sum_{i=1}^{d} \frac{n_i}{N_i} \tag{4}$$

Tables 6–8 show the total damage to the blade lever within one cycle under three contact conditions. According to Miner's theory, the entire life zone of the blade lever under fixed contact has 2.01×10^{31} cycles. The entire life zone of the blade lever under frictional contact has 6.49×10^{18} cycles. The entire life zone of the blade under frictionless contact has 7.24×10^{18} cycles. The life of fixed contact is 3.097×10^{12} times that of frictional contact and 2.776×10^{12} times that of frictional contact. There is a significant difference in the fatigue life prediction results of blade levers under three types of contact using Miner's cumulative damage theory. The life results of frictional contact and frictionless contact are similar, and both are much smaller than the life calculated by fixed contact.

Table 6. Damage degree of stress of blade lever under bonded contact condition.

σ_a	*n*	*N*	D (*n*/*N*)
0.01	18	6.05×10^{42}	2.98×10^{-42}
0.03	2	3.43×10^{38}	5.83×10^{-39}
0.195	3	1.59×10^{32}	1.88×10^{-32}

Table 7. Damage degree of stress of blade lever under frictional contact condition.

σ_a	*n*	*N*	D (*n*/*N*)
0.01	18	2.06×10^{20}	8.71×10^{-20}
0.03	2	1.01×10^{20}	2.98×10^{-20}
0.195	3	8.06×10^{19}	3.72×10^{-20}

Table 8. Damage degree of stress of blade lever under frictionless contact condition.

σ_a	*n*	*N*	D (*n*/*N*)
0.01	18	2.31×10^{20}	7.81×10^{-20}
0.03	2	1.12×10^{20}	2.67×10^{-20}
0.195	3	8.89×10^{19}	3.33×10^{-20}

7. Conclusions

In this article, the unsteady flow field is calculated and analyzed, and then the FSI is used to load the unsteady hydraulic load onto the runner. The runner operating mechanism is composed of a multi-body system using fixed contact, frictional contact, and frictionless contact methods. The dynamic stress of the runner is calculated. Then, the stress time history is calculated using the rain flow counting method to obtain an array of mean and amplitude stresses. Finally, the lifespan of the blade lever is calculated based on the lifespan curve. The following main conclusions have been drawn:

The torque of the six blades around the blade lever is unsteady, non-uniform, and asynchronous. This state of force and torque causes accelerated damage to the blade lever, and fatigue cracks gradually accumulate on the blade lever. The main frequency of pressure, torque, and structural stress pulsation is 1 fn, which is related to the rotation of the runner. This indicates that the rotation of the runner has a significant impact on the hydraulic and structural characteristics of the Kaplan turbine.

Under the combination of flow impact, gravity, and centrifugal force, the displacement of rotating components under the three contact conditions is mainly concentrated at the trailing edge of the blade. The displacement and fluctuation of the blade under frictional and frictionless contact are much larger than those under fixed contact.

Under fixed, frictional, and frictionless contact modes, the average stress of the blade is not significantly different, and the fluctuation amplitude is similar. But as the main force transmission component of the runner system, the blade lever has the highest average stress under frictional and frictionless contact conditions. Its maximum stress is between 305 MPa and 299 MPa, located at the junction of the blade lever and the hub. The blade lever stress under fixed contact mode is 19.6 MPa, which is much lower than that under the other two cases, located at the groove at the intersection of the blade lever and the inside of the runner body. Similar to the blade lever, the stress results of the runner body under the fixed contact condition are much smaller than those of frictional and frictionless contact, and its maximum stress is located at the junction of the blade and hub. The maximum stress position of the runner body under friction and frictionless contact is at the junction of the blade lever circumference surface and the hub of the runner body.

The lifespan of the blade lever under fixed contact conditions is 2.776×10^{12} times that under frictional and frictionless contact conditions, so the contact mode between the runner components has a significant impact on the structural lifespan.

Author Contributions: Conceptualization, Z.W. and L.Z.; methodology, C.L. and H.L.; investigation, C.L., G.W. and X.C.; validation, H.L. and C.L.; writing—original draft preparation, C.L. and G.W.; writing—review and editing, C.L., X.C. and H.L.; supervision, L.Z. and Z.W. All authors have read and agreed to the published version of the manuscript.

Funding: This work is supported by National Natural Science Foundation of China (No.: 51876099).

Data Availability Statement: The data presented in this study are available on request from the corresponding author.

Acknowledgments: The author sincerely thanks the project support: "Research on the Safe and Stable Operation of the Datongxia Large Kaplan Tubrbine Project" from Guangxi Datengxia Gorge Water Conservancy Development Co., Ltd.

Conflicts of Interest: Authors Haiqiang Luo, Guiyu Wang and Xiaobin Chen were employed by the company Guangxi Datengxia Gorge Water Conservancy Development Co., Ltd. The remaining authors declare that the research was conducted in the absence of any commercial or financial relationships that could be construed as a potential conflict of interest. The Guangxi Datengxia Gorge Water Conservancy Development Co., Ltd. had no role in the design of the study; in the collection, analyses, or interpretation of data; in the writing of the manuscript, or in the decision to publish the results.

References

1. Iovănel, R.G.; Bucur, D.M.; Cervantes, M.J. Study on the accuracy of RANS modelling of the turbulent flow developed in a Kaplan turbine operated at BEP. Part 1—Velocity field. *J. Appl. Fluid Mech.* **2019**, *12*, 1449–1461. [CrossRef]
2. Liu, S.; Mai, J.; Shao, J. Pressure pulsation prediction by 3D turbulent unsteady flow simulation through whole flow passage of Kaplan turbine. *Eng. Comput.* **2009**, *26*, 1006–1025. [CrossRef]
3. Altimemy, M.; Watheq, S.; Caspar, J. Performance of Kaplan Turbine Operating at Design Condition. In Proceedings of the Fluids Engineering Division Summer Meeting, Virtual Online, 10–12 August 2021; Volume 85307, p. V003T05A018.
4. Petit, O.; Mulu, B.; Nilsson, H. Comparison of numerical and experimental results of the flow in the U9 Kaplan turbine model. *IOP Conf. Ser. Earth Environ. Sci.* **2010**, *12*, 012024. [CrossRef]
5. Puolakka, O.; Keto-Tokoi, J.; Matusiak, J. Unsteady load on an oscillating Kaplan turbine runner. *J. Fluids Struct.* **2013**, *37*, 22–23. [CrossRef]
6. Liu, X.; Presas, A.; Luo, Y. Crack growth analysis and fatigue life estimation in the piston rod of a Kaplan hydro turbine. *Fatigue Fract. Eng. Mater. Struct.* **2018**, *41*, 2402–2417. [CrossRef]
7. Wang, Z.W.; Luo, Y.Y.; Zhou, L.J. Computation of dynamic stresses in piston rods caused by unsteady hydraulic loads. *Eng. Fail. Anal.* **2008**, *15*, 28–37. [CrossRef]
8. Zhou, L.J.; Wang, Z.W.; Xiao, R.F. Analysis of dynamic stresses in Kaplan turbine blades. *Eng. Comput.* **2007**, *24*, 753–762. [CrossRef]
9. Urquiza, G.; Garcia, J.C.; Gonzalez, J.G. Failure analysis of a hydraulic Kaplan turbine shaft. *Eng. Fail. Anal.* **2014**, *41*, 108–117. [CrossRef]
10. Kan, K.; Zheng, Y.; Fu, S. Dynamic stress of impeller blade of shaft extension tubular pump device based on bidirectional fluid–structure interaction. *J. Mech. Sci. Technol.* **2017**, *31*, 1561–1568. [CrossRef]
11. Luo, Y.; Wang, Z.; Zeng, J. Fatigue of piston rod caused by unsteady, unbalanced, unsynchronized blade torques in a Kaplan turbine. *Eng. Fail. Anal.* **2010**, *17*, 192–199. [CrossRef]
12. Xu, J.; Lei, D.; He, J. Torque characteristics of guide vanes protection device of Francis turbine in hydropower plant. *Eng. Fail. Anal.* **2021**, *127*. [CrossRef]
13. Wang, H.T. The Analysis of Cracks in Axial Flow Fixed Paddle-type Vane. *Heavy Cast. Forg.* **2007**, *4*, 38–39.
14. David, F.; Neil, B.; Bede G. Fitness for purpose assessment after an over pressure incident at Arapuni Power Station. *Int. J. Press. Vessel. Pip.* **2004**, *81*, 471–479.
15. Shigley, J.E.; Mischke, C.R. *Mechanical Engineering Design*; McGraw-Hill: New York, NY, USA, 1989.
16. Sines, G.; Ohgi, G. Fatigue criteria under combined stresses or strains. *J. Eng. Mater. Technol.* **1981**, *103*, 82–90. [CrossRef]
17. Davis, E.A.; Connelly, F.M. Stress distribution and plastic deformation in rotating cylinders of strain-hardening material. *J. Appl. Mech.* **1959**, *18*, 25–30. [CrossRef]
18. Manson, S.S.; Halfordand, G.R. Discussion to the paper "Multiaxial low cycle fatigue of type 304 stainless steel" by J. J. Blass and S. Y. Zamrik. *J. Eng. Mater. Technol.* **1977**, *99*, 283–285. [CrossRef]
19. Kallmeyer, A.R.; Krgo, A.; Kurath, P. Evaluation of multiaxial fatigue life prediction methodologies for Ti-6Al-4V. *J. Eng. Mater. Technol.* **2002**, *124*, 229–237. [CrossRef]
20. Chang, J.B.; Hudson, C.M. *Methods and Models for Predicting Fatigue Crack Growth under Random Loading*; ASTM International: West Conshohocken, PA, USA, 1981; pp. 115–132.
21. Salam, I.; Abid, M.; Malik, M.A. Crack growth prediction in a thick cylinder under fatigue loading-an FEA. *Int. J. Syst. Appl. Eng. Dev.* **2007**, *3*, 51–53.
22. Jürgen, S. Experimental investigation of the rim-lip-seal of a double regulated STRAFLO Kaplanturbine under extreme conditions. In *Promoting the Versatile Role of Hydro, Proceedings of the Hydro—International Conference and Exhibiton, Innsbruck, Austria, 7–9 October 2013*; Aqua Media International Ltd.: Carshalton, UK, 2013.
23. Terentiev, L. *The Turbulence Closure Model Based on Linear Anisotropy Invariant Analysis*; Friedrich-Alexander-Universitaet Erlangen-Nuernberg (Germany), ProQuest Dissertations Publishing: Erlangen, Germany, 2006.
24. Menter, F.; Rumsey, C. Assessment of two-equation turbulence models for transonic flows. In Proceedings of the Fluid Dynamics Conference, Colorado Springs, CO, USA, 20–23 June 1994; pp. 1–18.
25. Bathe, K.J. *Finite Element Procedures*; Klaus-Jurgen Bathe: Cambridge, MA, USA, 2006.